Electronic Supplementary Material (ESI) for ChemComm.

Electronic Supporting Information

Multiple Energy Dissipation Modes in Dynamic Polymer Networks with Neutral and Ionic Junctions

Seongon Jang[†,‡,§], Charles M. Schroeder[†,‡,§,‖], Christopher M. Evans*[,†,‡,§,‖]

[†]Department of Materials Science and Engineering, [‡]Materials Research Laboratory, [§]Beckman Institute for Advanced Science and Technology, [‖]Department of Chemical and Biomolecular Engineering, University of Illinois at Urbana-Champaign, Urbana, Illinois 61801, United States

*Corresponding author, email: cme365@illinois.edu

1. Materials

Lithium hydroxide monohydrate ($LiOH \cdot H_2O$, 99%) and boric acid ($B(OH)_3$, 99.5%) were purchased from Sigma-Aldrich. Hexaethylene glycol (6EG, 99%) was purchased from AK Scientific. Methyl alcohol (MeOH, anhydrous) was purchased from Macron Fine Chemicals. Purchased chemicals were used without further purification.

2. Dynamic network synthesis

$B(OH)_3$ (1 eqv), 6EG (1.5 + [LiOH] eqv) and LiOH were mixed in a Schlenk flask at room temperature under nitrogen purging with a needle. After adding 5 mL of anhydrous MeOH, the mixture was heated at 60 ℃ and stirred for 2 hours until a clear homogenous solution was achieved. Next, a nitrogen line was connected to the Schlenk flask and allowed to continuously flow through a vent port. The temperature increased gradually to 70 ℃ for 2 hours, 120 ℃ for 2 hours, and 150 ℃ overnight. Lastly, the flask was dried under vacuum at 120 ℃ overnight to remove water and cure completely, resulting in transparent brown solids. Subsequently, all samples were transferred into glovebox and stored before further characterization. The as-synthesized vitrimers are named as B-6EG or B-6EG-x, where x indicates the percent of boron sites that are ionic in polymer networks. Neutral vitrimers were synthesized with the same procedure without adding salts.

3. Methods

Solid-state NMR. ^{11}B solid-state NMR spectra were obtained using a Varian Unity Inova 300 MHz spectrometer. Samples were densely packed inside 4 mm ceramic rotors in a glovebox and measured with a magic angle spinning (MAS) speed of 10 kHz with 10000 total scans. MNOVA software was used to determine chemical shifts and assign peaks for the collected spectra.

ATR-FTIR. Infrared spectra were obtained using a Bruker ALPHA FT-IR spectrometer equipped with platinum-ATR QuickSnap sampling module. All samples were measured inside of Argon glovebox to prevent decomposition by moisture. The scanning range is from 4000 cm^{-1} to 400 cm^{-1} with 32 scans and 4 cm^{-1} resolution.

Differential Scanning Calorimetry (DSC). DSC measurements were performed on a TA Instruments DSC 2500 instrument. Samples weighing between 8-10 mg were sealed in DSC aluminum hermetic pans inside of a glovebox. Subsequently, the samples were subjected to a heat/cool/heat cycle in a temperature range from -150 ℃ to 120 ℃ for all samples with a rate of 10 ℃/min. The glass transition temperature T_g was determined using the ½ ΔC_p criterion from the second heating cycle.

Thermogravimetric Analysis (TGA). The thermal stability of the polymer samples was assessed using a TA Instruments Q50. All samples were prepared by sealing samples (8-10 mg) in hermetic aluminum pans in Ar glovebox. Before each measurement, a hole was generated in the lid of the

pan using a 22-gauge needle. Each sample was heated from 30 ℃ to 500 ℃ at a rate of 10 ℃/min under N_2.

Rheology. Rheological characterization experiments were performed using a TA Instruments DHR-2 rheometer outfitted with an environmental control chamber and 8 mm stainless steel parallel plates. Before each measurement, samples were prepared into a circular geometry of 8 mm diameter using a PTFE washer at 120 ˚C in Ar glovebox. The samples were quickly loaded onto the rheometer plates pre-heated at 120 ˚C and heated for 30 min to remove any potential H_2O that could be adsorbed onto the surface during the loading process. The thickness of disc samples was about 900 μm. An amplitude sweep was then conducted at 120 ˚C from 0.1 to 10% strain to determine linear viscoelastic regimes. Temperature ramps were performed by heating from -60 ˚C to 120 ˚C at a rate of 2 ˚C/min at 0.5 Hz with a controlled stress of 1000 Pa. The lowest temperatures varied depending on the concentration of lithium hydroxide which changed the glass transition temperature of the networks. Oscillatory shear linear viscoelastic (LVE) experiments were measured from 100 rad/s to 0.01 rad/s at 20 ˚C intervals from 120 ˚C to -20 ˚C. The crossover time τ was defined as the time where shear storage (G') and loss (G") moduli have same value. These crossover times were plotted as a function of 1000/T and fit to Arrhenius equation, which provides the activation energy for flow. The relaxation spectra in this paper were obtained using TRIOS software. The LVE data was fitted to a regularized high-density continuous spectrum. It was confirmed that the number of data points for fitting did not affect the results. The dynamic moduli are computed as described in the supplementary data (Fig. S7). The spectra were trimmed by Anderssen and Davies criteria as $\frac{e^{\pi/2}}{\omega_{max}} < \tau < \frac{e^{-\pi/2}}{\omega_{min}}$.

WAXS. The morphology of the vitrimers was characterized using a Xenocs GeniX3D Cu Kα X-ray source (1.54Å) with a Pilatus 2D detector. A road beam stop is positioned in front of the detector to dampen the primary beam. The sample-to-detector distance was calibrated using silver behenate powder. To prevent the samples from decomposing due to moisture, the samples were packed in a 1 mm thick quartz capillary tube under Ar environment and sealed with marine epoxy (Devcon, home 5 Minute Epoxy). All measurements were collected under ambient conditions with 60-minute exposure time. The 2D diffraction data was processed using FIT2D software to obtain plots of intensity versus scattering vector.

4. Supplementary data

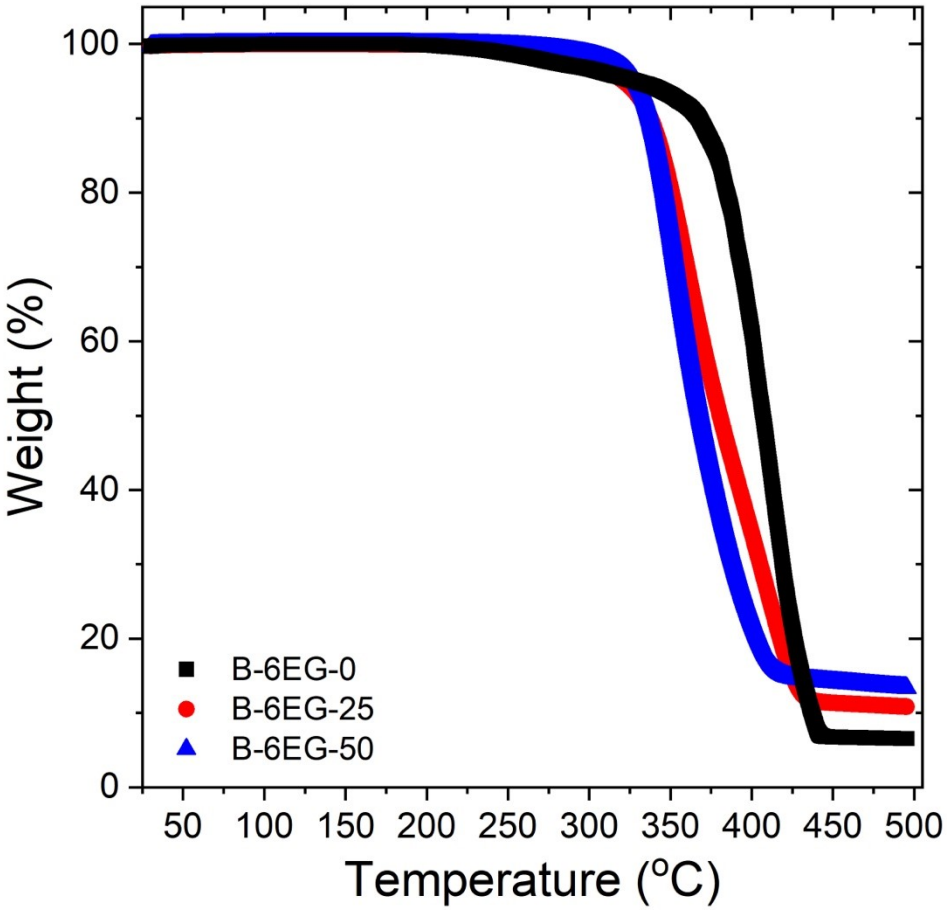

Figure S1. TGA analysis of the samples under nitrogen environment. Degradation time T_d decreased upon adding salt. Vitrimers with salt exhibited higher remaining weight percentage at high temperature because of residual oxidized salt compared to neutral vitrimers.

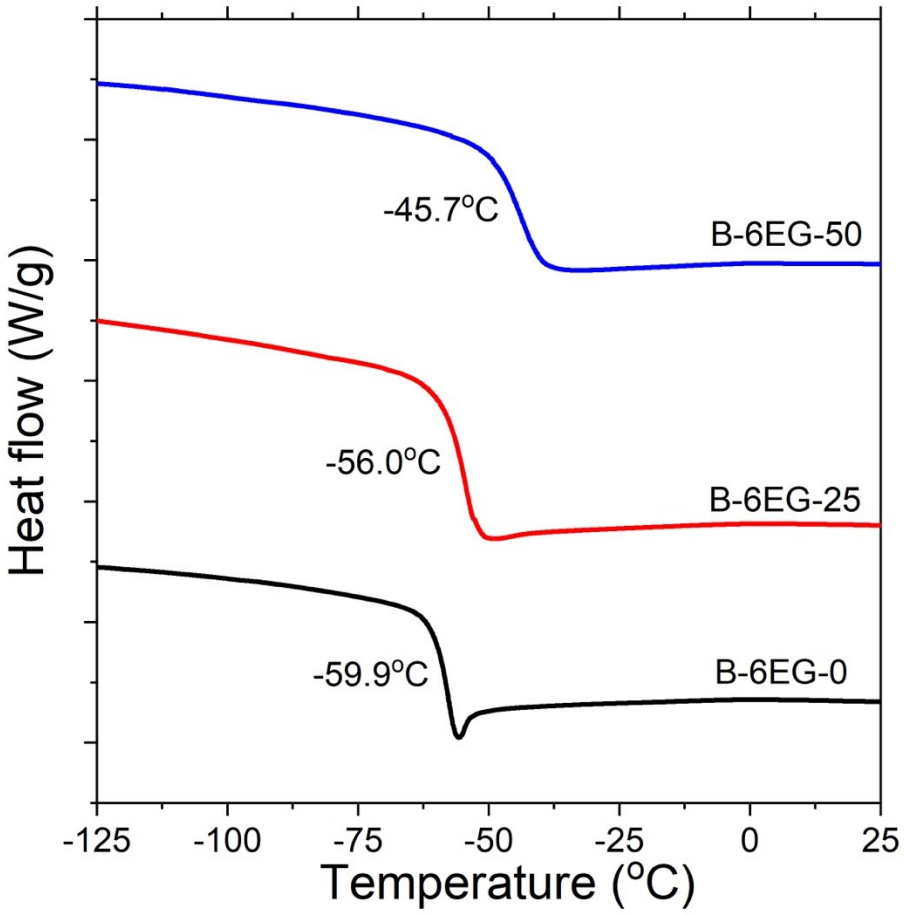

Figure S2. Second heating DSC curves for neutral and ionic vitrimers. The T_g was determined using the midpoint at half height method. The T_g of vitrimers was observed to increase upon adding salts due to higher crosslinking density of ionic/tetragonal crosslinkers.

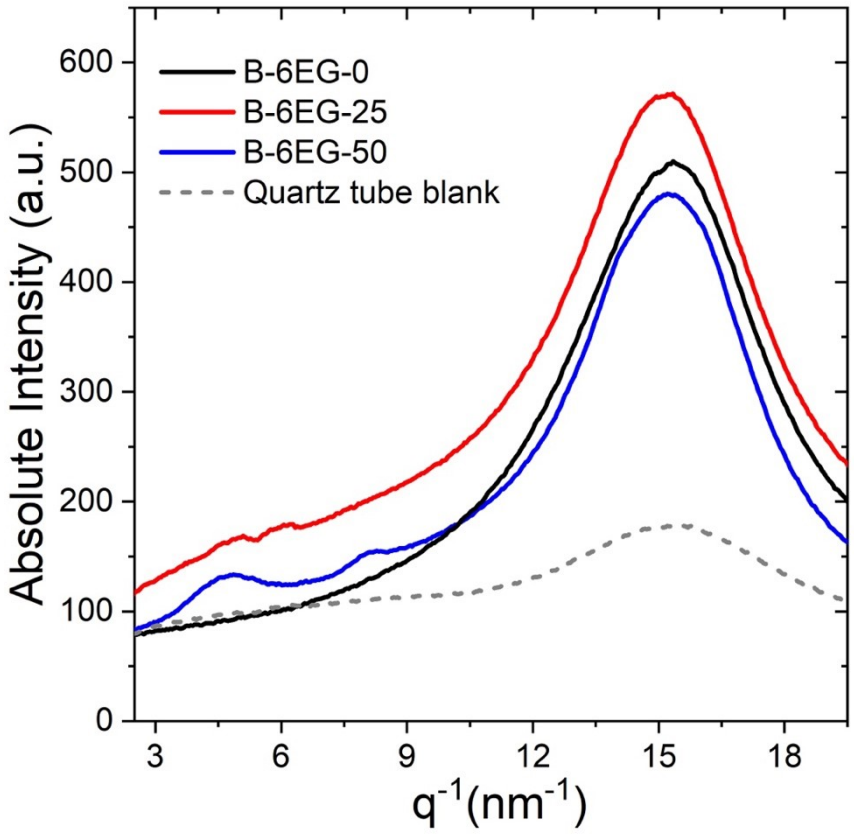

Figure S3. WAXS (wide-angle X-ray scattering) data for blank quartz tube and vitrimer with different ratio of ionic junctions.

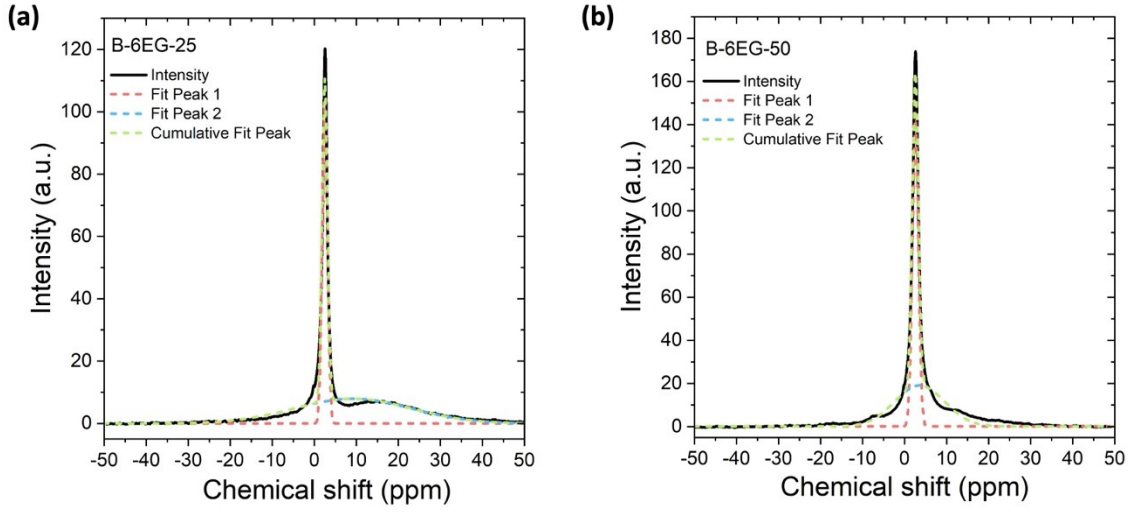

Figure S4. ^{11}B solid-state NMR with deconvolution analysis of vitrimers with neutral and ionoic sites.

B-6EG-25	ppm	Area	Molar Percentage
Neutral junction	15.6	8979	72.3%
Ionic junction	2.55	3440	27.7%
B-6EG-50	**ppm**	**Area**	**Percentage**
Neutral junction	15.2	7718	49.1%
Ionic junction	2.60	7990	50.9%

Table S1. Fitted parameters for deconvolution of ^{11}B ssNMR.

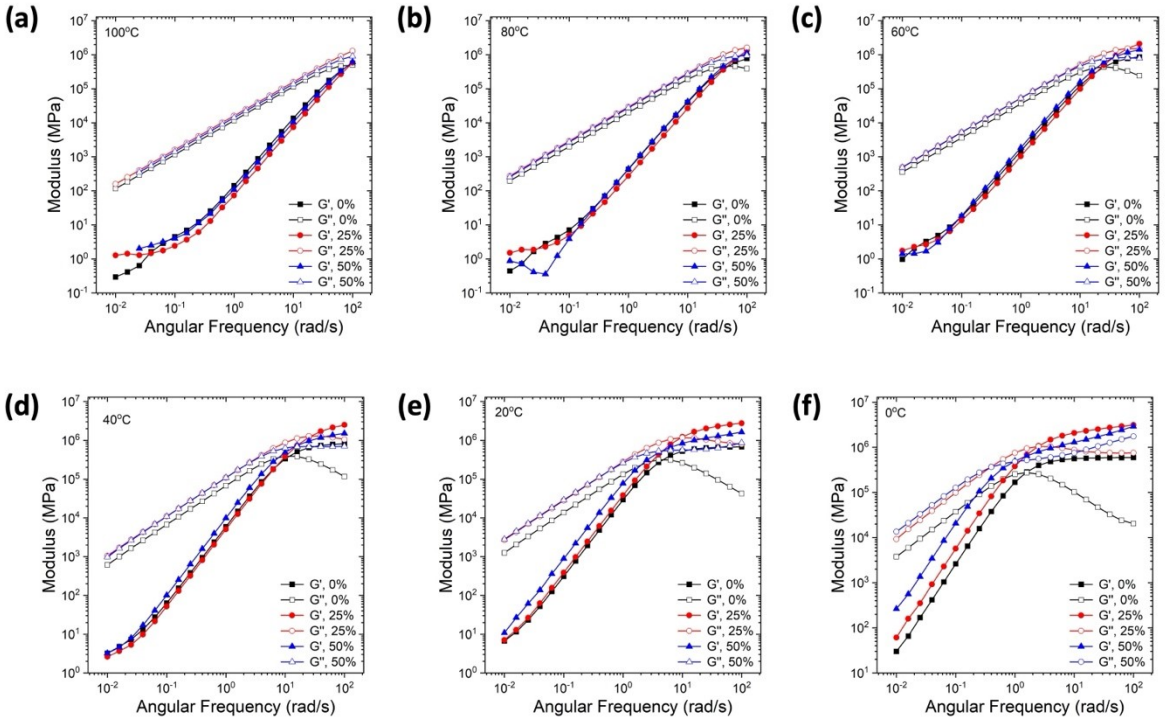

Figure S5. Dynamic oscillatory linear viscoelastic data for all vitrimers from 100℃ to 0℃. (Black, B-6EG-0/Red, B-6EG-25/Blue, B-6EG-50)

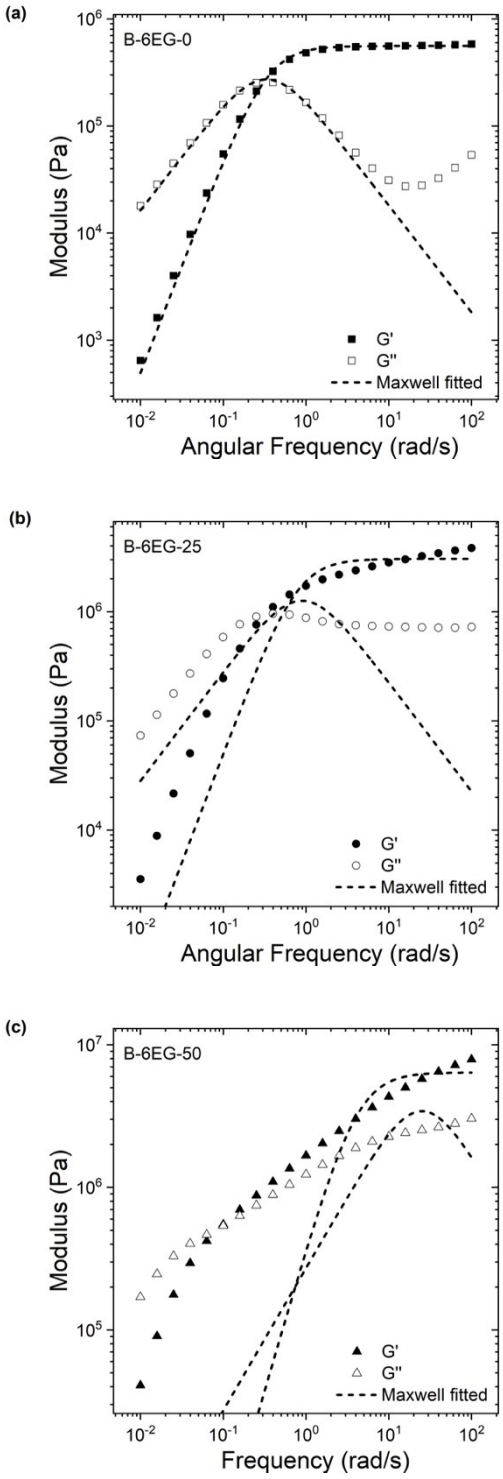

Figure S6. (a) B-6EG-0 exhibits typical Maxwell behavior, and its relaxation behavior can be described with a single mode. (b) B-6EG-25 and (c) B-6EG-50 cannot be fitted with single-mode Maxwell models. The poor fit indicates that the model neither captures the crossover nor the second dominant mode at higher frequeny.

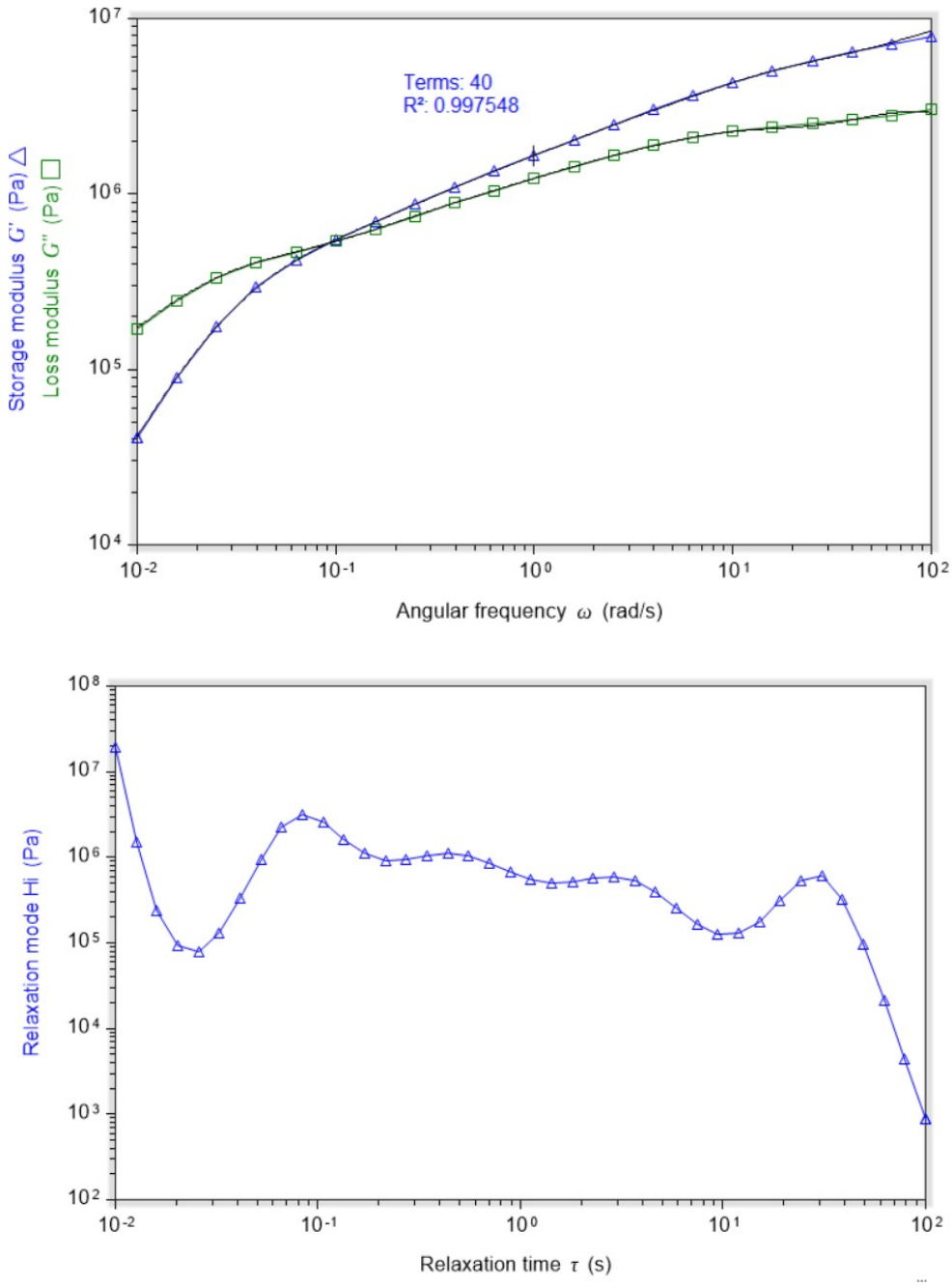

Figure S7. Analysis of dynamic oscillatory linear viscoelastic (LVE) data by fitting to a regularized high-density continuous spectrum through TRIOS software. The dynamic moduli (G' and G'') are fitted using below equations, which converts to a Riemann sum. The regularized fit minimizes the error between the data and spectrum prediction and ensures smoothness and continuity of the relaxation spectrum by regularizing metric.

$$G'(\omega) = \sum_i H_i \log\left(\frac{\tau_{i+1}}{\tau_i}\right)\frac{(\omega\tau_i)^2}{1+(\omega\tau_i)^2},\quad G''(\omega) = \sum_i H_i log(\frac{\tau_{i+1}}{\tau_i})\frac{\omega\tau_i}{1+(\omega\tau_i)^2}$$

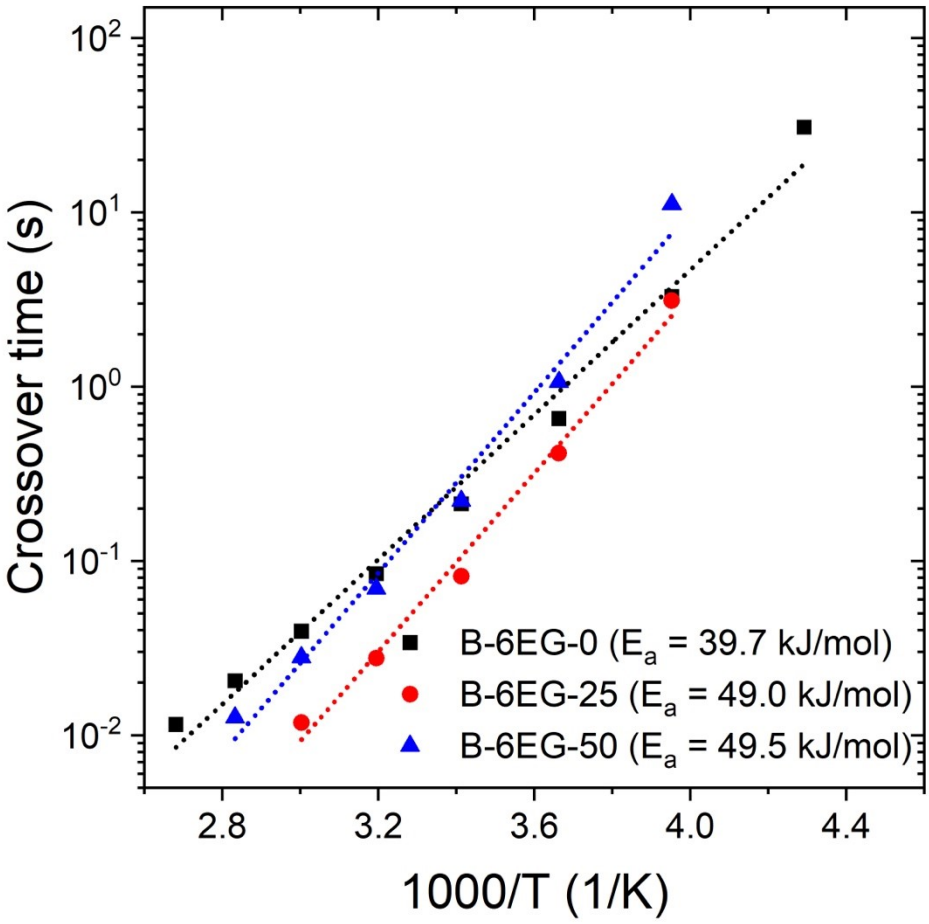

Figure S8. Arrhenius plot for B-6EG-0, B-6EG-25, and B-6EG-50. The activation energies are calculated from the slope of the crossover time versus inverse temperature.

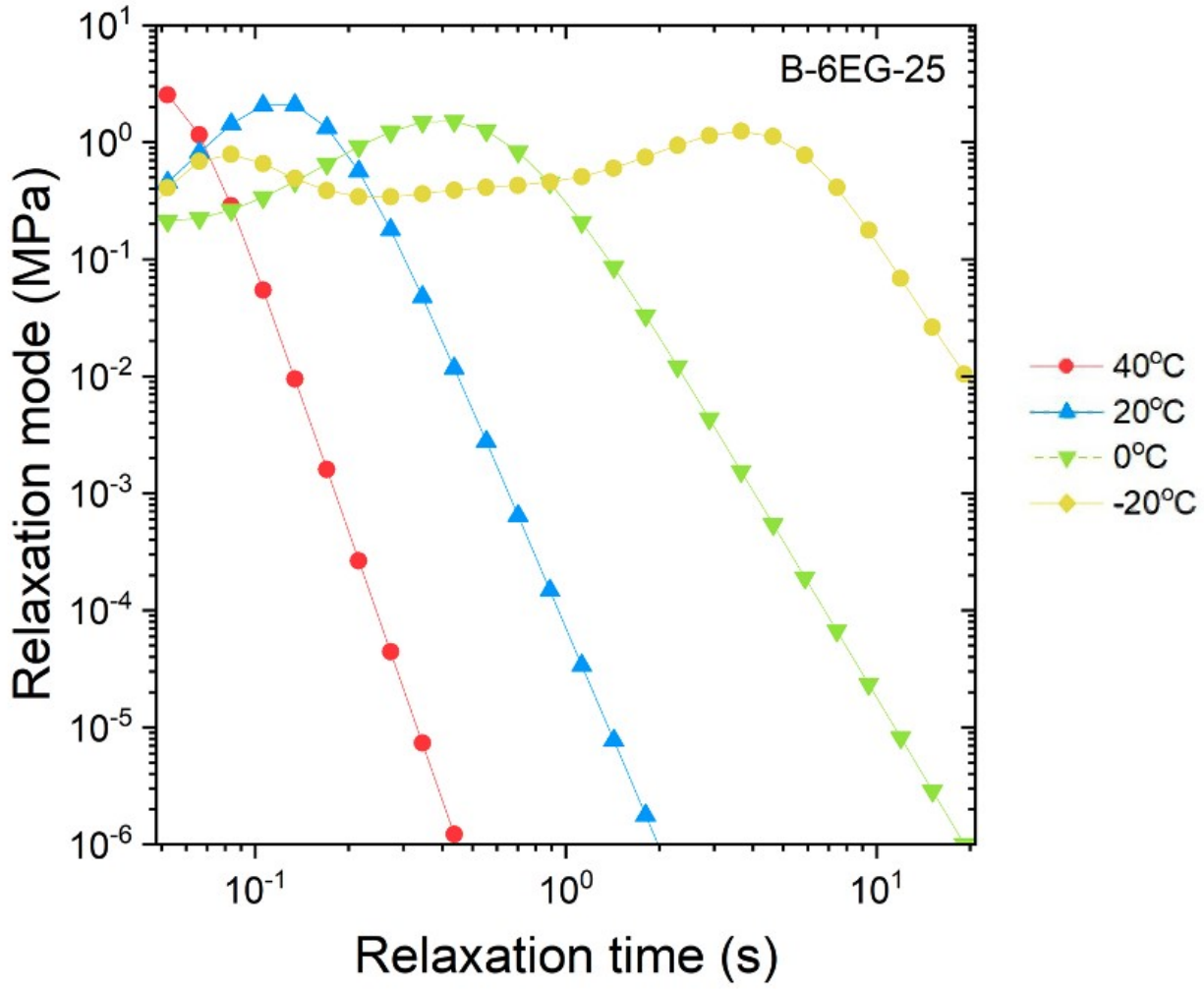

Figure S9. Relaxation time spectrum at various temperatures for boronic-ester vitrimers with 25% ionic junction composition.

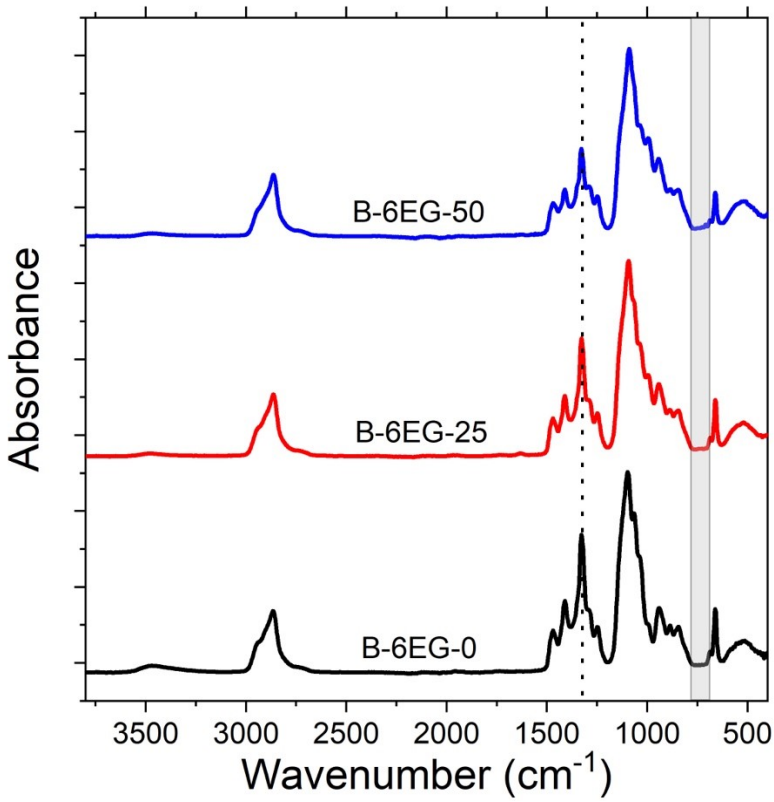

Figure S10. ATR-FTIR spectra of neutral and ionic vitrimers. Peaks around 1330cm-1 are characteristic peaks of boronic ester (B-O) bonds, which have been reported in same ethylene glycol linker-based boronic ester vitrimers.[1] No peaks are observed in 750 cm-1 region, corresponding to boroxine bonds (B3O3).[2]

	$B(OH)_3$	6EG	LiOH
0% ionic sites	2 eqv	3 eqv	0 eqv
25% ionic sites	2 eqv	3.5 eqv	0.25 eqv
50% ionic sites	2 eqv	4 eqv	0.5 eqv

Table S2. Stoichiometry calculation for synthesis of neutral and ionic vitrimers.

(a)

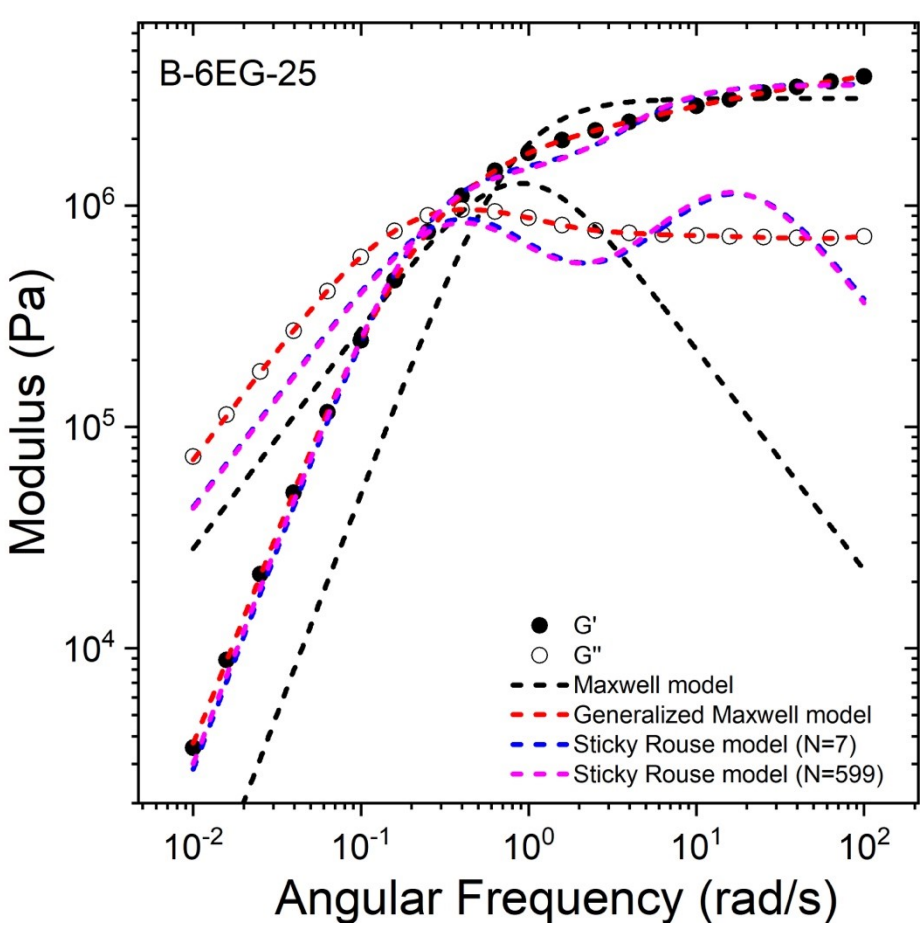
B-6EG-25
Modulus (Pa)
10^6
10^5
10^4
10^{-2}
10^{-1}
10^0
10^1
10^2
Angular Frequency (rad/s)
G'
G''
Maxwell model
Generalized Maxwell model
Sticky Rouse model (N=7)
Sticky Rouse model (N=599)

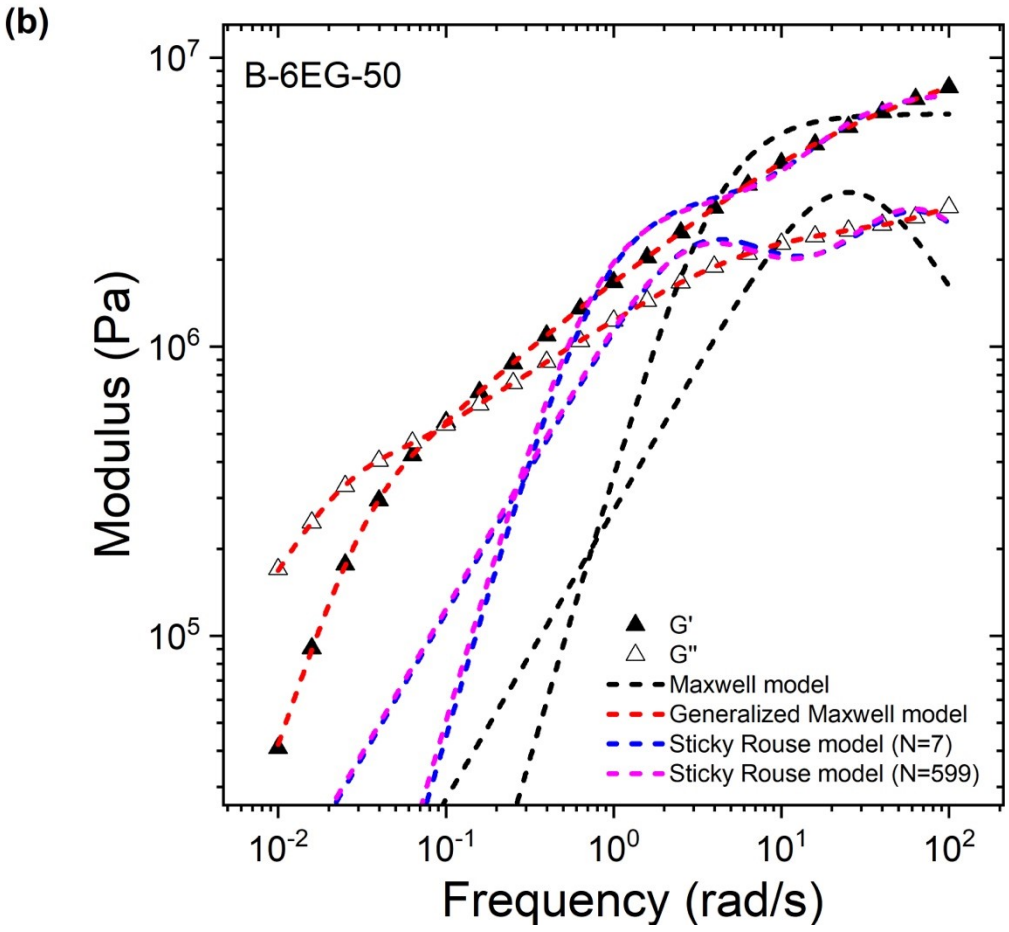

Figure S11. Analysis of experimental data using a single, generalized Maxwell and sticky Rouse model fits to shear rheology data at -20℃ for (a) B-6EG-25 and (b) B-6EG-50 vitrimers.

We appreciate the reviewer's suggestion to consider using the sticky Rouse model to explain the relaxation behavior of the vitrimers. The sticky Rouse model has been used to analyze the viscoelastic behavior of associative polymers with hydrogen bonding[3] and ionomers[4]. There is only one prior study in the literature in which the sticky Rouse model was used to describe the viscoelasticity of unentangled vitrimers. In general, the reversible bonds (stickers) slow down the relaxation of the polymer chains if their relaxation time scale is longer than that predicted by the standard Rouse model.

The equations for storage and loss moduli from the sticky Rouse model are given by Equations 1 and 2, respectively (see below). In the expressions for storage and loss moduli, the first summation represents slow sticky modes attributed to dynamic bond exchange at neutral and ionic crosslinking sites. The second summation includes the standard Rouse modes for the polymer chains, which are typically faster than the sticky Rouse modes. In applying the sticky Rouse model, several assumptions are made to validate the fitting process for our vitrimer materials: (1) Crosslinking sites/bonds are fully saturated, and there are no unreacted bonding sites. (2) The polymer networks are homogeneous.

$$G'(\omega) = G\left[\sum_{i=1}^{N_x-1}\frac{{\tau_1}^2\omega^2}{1+{\tau_1}^2\omega^2} + \sum_{i=N_x}^{N}\frac{{\tau_1}^2\omega^2}{1+{\tau_1}^2\omega^2}\right] \quad (1)$$

$$G''(\omega) = G\left[\sum_{i=1}^{N_x-1}\frac{\tau_1\omega}{1+{\tau_1}^2\omega^2} + \sum_{i=N_x}^{N}\frac{\tau_2\omega}{1+{\tau_2}^2\omega^2}\right] \quad (2)$$

In the above equations, the number of standard Rouse modes N and the number of sticky Rouse modes (crosslinking sites) N_x are selected based on prior literature[5]. The results are shown in Figure S11.

We anticipate that the sticky Rouse model cannot fully capture the multi-modal relaxation behavior of the ionic vitrimers due to the following reasons. First, our dynamic polymer networks differ qualitatively from polymer materials typically described using Rouse model. Our vitrimers consist of very short hexaethylene glycol (6EG) chains, so in the absence of dynamic bonds, the material is only comprised of short oligomers and not polymer chains. Therefore, in the absence of dynamic bonding, our materials have no intrinsic Rouse modes because there are no polymer chains. This violates a basic assumption of the sticky Rouse model, which assumes that long polymer chains exist (and show appreciable Rouse nodes) in the absence of intermolecular associations. Additionally, our vitrimers are entirely formed by multiple bond exchange sites (e.g., neutral, ionic, and ionic clusters), each with distinct relaxation time scales. As shown in Figure R2, even though we increased the number of modes from 7 to 599, the sticky Rouse model still failed to fit the data. However, the generalized Maxwell model could perfectly fit the data with only seven modes. Another reason is the intrinsic inhomogeneity of the polymers. In WAXS, our results show clear evidence of aggregation of ionic crosslinking sites. In prior work relying on the sticky Rouse model[5], the authors explicitly mention that the sticky Rouse model may not be appropriate if the polymer material is highly non-homogeneous, which is likely the case for our polymer materials. To clarify these points, we added figures, tables, and statements in SI (Figure S11, Table S3) on pages 13-16.

$$G'(\omega) = G_\infty + \sum_{i=1}^{n} G_i\frac{{\tau_i}^2\omega^2}{1+{\tau_i}^2\omega^2} \quad (3)$$

$$G''(\omega) = \sum_{i=1}^{n} G_i\frac{\tau_i\omega}{1+\tau_i^2\omega^2} \quad (4)$$

* Generalized Maxwell model when n = 7

(a) Sticky Rouse model (N = 599 or 7)

B-6EG-25	G (Pa)	τ_1 (Relxation time of sticky Rouse mode)	τ_2 (Relaxation time of standard Rouse mode)	N (Number of Rouse modes)	N_x (Number of sticky Rouse modes,

					Crosslinking sites)
Storage	5844	4.55	0.21	599	249
Loss	6314	2.64	0.06	599	249

B-6EG-50	G (Pa)	τ_1 (Relxation time of sticky Rouse mode)	τ_2 (Relaxation time of standard Rouse mode)	N (Number of Rouse modes)	N_x (Number of sticky Rouse modes, Crosslinking sites)
Storage	12615	1.28	0.05	599	249
Loss	15881	0.29	0.01	599	249

B-6EG-25	G (Pa)	τ_1 (Relxation time of sticky Rouse mode)	τ_2 (Relaxation time of standard Rouse mode)	N (Number of Rouse modes)	N_x (Number of sticky Rouse modes, Crosslinking sites)
Storage	503624	4.33	0.19	7	4
Loss	545829	2.57	0.05	7	4

B-6EG-50	G (Pa)	τ_1 (Relxation time of sticky Rouse mode)	τ_2 (Relaxation time of standard Rouse mode)	N (Number of Rouse modes)	N_x (Number of sticky Rouse modes, Crosslinking sites)
Storage	1080184	1.18	0.05	7	4
Loss	1359485	0.27	0.01	7	4

(b) Generalized Maxwell model (n=7)

B-6EG-25	G_∞ (Pa)	G1 (Pa) tau1 (s)	G2 (Pa) tau2 (s)	G3 (Pa) tau3 (s)	G4 (Pa) tau4 (s)	G5 (Pa) tau5 (s)	G6 (Pa) tau6 (s)	G7 (Pa) tau7 (s)
Storage	331	586283 0.14	448292 0.49	679534 0.01	546677 0.04	605530 1.46	991060 3.54	296083 8.25
Loss	-	602360 0.98	565400 0.24	1079487 0.005	486409 6.68	501023 0.02	1044006 2.93	525090 0.07

B-6EG-50	G_∞ (Pa)	G1 (Pa) tau1 (s)	G2 (Pa) tau2 (s)	G3 (Pa) tau3 (s)	G4 (Pa) tau4 (s)	G5 (Pa) tau5 (s)	G6 (Pa) tau6 (s)	G7 (Pa) tau7 (s)
Storage	4530	471159 5.35	470944 28.7	2493848 0.01	1999926 0.04	1148747 0.41	773142 1.47	1716877 0.14
Loss	-	780688 1.44	1333099 0.38	461472 28.8	1942565 0.11	5304455 0.005	2112112 0.033	476936 5.43

Table S3. (a) Sticky Rouse model and (b) generalized maxwell model fitting parameters for storage and loss modulus of B-6EG-25 and B-6EG-50 vitrimers.

Reference

[1] B. B. Jing, P. Mata, Q. Zhao, C. M. Evans, Journal of Polymer Science, 2021, 59, 1-10.

[2] L. Wan, X. Du, L. Guo, X. Tan, Y. Tong, D. Zhou, C. Liu, Y. Qin, G. Zheng, Journal of Energy Storage, 2023, 74, 109485.

[3] N. Jiang, H. Zhang, P. Tang, Y. Yang, Macromolecules, 2020, 53, 3438-3451.

[4] Q. Chen, G. J. Tudryn, R. H. Colby, Journal of Rheology, 2013, 57, 1441-1462.

[5] R. G. Ricarte, S. Shanbhag, Macromolecules, 2021, 54, 3304-3320.